CHAPTER – 5

PHOTONIC BAND GAP AND LOCALIZATION MODE ANALYSIS IN ONE-DIMENSIONAL QUASI-PERIODIC PHOTONIC CRYSTALS

5.1 Introduction

With unusual and intriguing the properties of electromagnetic wave propagation, great efforts have been dedicated towards the investigation of the photonic band gap (PBG) properties in quasi-periodic systems after the discovery of the quasi-crystalline structure [Albuquerque (2003); Lahini (2009); Mahler (2010)]. Quasi-periodic arrangements are fixed in a regular pattern and follow a simple deterministic recursion rule [Steurer (2009); Poddubny (2010)]. Quasi-periodic systems are one of the most interesting arrangements to obtain the suitable PBGs because of several structural parameters available to tune as compared to the periodic and disordered systems. Recently, some research groups have been reported their works on electromagnetic wave propagation in quasi-periodic structures that known as photonic quasicrystals [Negro (2005); Vardeny (2013); Negro (2014)]. These structures provide a range of technological application in several fields [Man (2005); Rechtsman (2008); Freedman (2006)]. The PBG properties of quasi-periodic multi-layered structures have been extensively studied for different materials such as dielectric, metallic and negative refractive index materials etc. [Vasconcelos (2007); Entezar (2009); Thiem (2011); Macia (2012)]. Specifically, one-dimensional (1-D) PQCs are very important because their formation is relatively easy, and which provide the description of light propagation in one direction [Ghulinyan (2005); Coelho (2010); Trabelsi (2013)]. 1-D PQCs are composed of layers according to substitutional quasi-periodic sequences such as Fibonacci, Thue-Morse and Double-Periodic etc. These structures offer the benefit of the tunability of photonic and omnidirectional band gaps, self-similarity transmission spectral properties and localization phenomenon [Abdelaziz (2005); Nava (2009); Deng (2010); Coelho (2010); Rahimi (2011); Zhizhong (2012)].

In all the previous studies on optical properties in 1-D PQCs have been considered with different materials under different conditions but the uses of graded materials and

semiconductor in quasi-periodic structures are untouched. In the previous chapters of this thesis, we have investigated the PBG properties in the periodic PC structures with graded index and dispersive materials. We observed that the relative parameters of the constituted graded index and dispersive materials in the periodic PC structures have great influence to tune and control the photonic band gaps.

Motivated by the optical characteristics of the quasi-periodic systems, and constituted graded and dispersive materials in the periodic PC structures, we have presented the theoretical study of the effect of graded and semiconductor materials on the PBG properties in 1-D quasi-periodic PC structures in this chapter. The aim of this work is to tune the PBGs and localization modes and obtain the high reflectance through 1-D quasi-periodic PC structures composed of graded materials and semiconductor. Main attention is paid to the influence of geometrical parameters, grading profile, temperature and different quasi-periodic sequences and generations on the PBGs and localization modes. The quasi-periodic structures follow the Fibonacci (FB), Thue-Morse (TM) and Double-periodic (DP) substitutional sequences and generated by the following inflation rules: A→AB, B→A (FB); A→AB, B→BA (TM); and A→AB, B→AA (DP), where A and B are the building blocks modelling of different materials. The plan of this chapter is as follows. In section 5.2, the theoretical models and calculations of the reflectance, transmittance and band structure of the quasi-periodic PC structures with graded index materials and semiconductor are provided. Section 5.3 is devoted to the discussion of the reflection spectra and dispersion relation at different structural parameters, grading profile parameters, temperature and generations of the Fibonacci, Thue-Morse and Double-periodic sequences. Here, our study has been carried out in two parts. First, the influences of graded index materials on the PBGs and localization modes in 1-D quasi-periodic PC structures have investigated. Next, the effects of constituted semiconductor on photonic and omnidirectional band gaps in 1-D quasi-periodic PCs have demonstrated. Conclusions are presented in the last section.

5.2 Theoretical Description

In this work, we have considered the multilayer structures composed of two types of layers A and B. The stacks of two layers are arranged according to the recursion rule of the Fibonacci (FB), Thue-Morse (TM) and Double-Periodic (DP) sequences. These sequences are based on the two-letter alphabet (A, B) so the substitution rule: σ (A) =

AB, σ (B) = A (FB); σ (A) = AB, σ (B) = BA (TM); and σ (A) = AB, σ (B) = AA (DP). The substitution rule can also be written in the form of following matrix equations for FB, TM and DP, respectively: [Steurer (2009); Poddubny (2010)]

$$\boldsymbol{\sigma}: \begin{pmatrix}\mathbf{A}\\ \mathbf{B}\end{pmatrix} \rightarrow \begin{pmatrix}\mathbf{1} & \mathbf{1}\\ \mathbf{1} & \mathbf{0}\end{pmatrix}\begin{pmatrix}\mathbf{A}\\ \mathbf{B}\end{pmatrix} = \begin{pmatrix}\mathbf{AB}\\ \mathbf{A}\end{pmatrix}; \quad \ldots \quad \textbf{(FB)}$$

$$\boldsymbol{\sigma}: \begin{pmatrix}\mathbf{A}\\ \mathbf{B}\end{pmatrix} \rightarrow \begin{pmatrix}\mathbf{1} & \mathbf{1}\\ \mathbf{1} & \mathbf{1}\end{pmatrix}\begin{pmatrix}\mathbf{A}\\ \mathbf{B}\end{pmatrix} = \begin{pmatrix}\mathbf{AB}\\ \mathbf{BA}\end{pmatrix}; \quad \ldots \quad \textbf{(TM)}$$

$$\text{and } \boldsymbol{\sigma}: \begin{pmatrix}\mathbf{A}\\ \mathbf{B}\end{pmatrix} \rightarrow \begin{pmatrix}\mathbf{1} & \mathbf{1}\\ \mathbf{2} & \mathbf{0}\end{pmatrix}\begin{pmatrix}\mathbf{A}\\ \mathbf{B}\end{pmatrix} = \begin{pmatrix}\mathbf{AB}\\ \mathbf{AA}\end{pmatrix}; \quad \ldots \quad \textbf{(DP)}$$

On the basis of the above substitution rule, the first few generations of the sequences are listed in panels (i), (ii) and (iii) of table 5.1. The proposed multilayer structures consist of two kinds of media A and B. One is homogeneous layer (A) with refractive index equal to 1.5 and the other is graded materials with space dependent refractive index (1.5 to 4.1) or semiconductor with frequency and temperature dependent refractive index as the case considered for the medium B. The variation of refractive index in the graded medium is taken along the direction of layer thickness. The direction of wave propagation is considered along x-axis i.e. the direction normal to the stacked of layers, and the considered materials are assumed as nonmagnetic.

First, medium B considered as a graded index materials. The refractive indices of the considered graded layers vary in a linear and exponential fashion between the refractive index at initial (n_i) and final (n_f) values as; $\left[n_L(x) = n_i + \frac{(n_f - n_i)}{d_2} \times x\right]$ and $\left[n_E(x) = n_i.exp\left(\frac{x}{d_2}.\log\frac{n_f}{n_i}\right)\right]$, respectively. Here, d_2 is the thickness of layers B. Next, medium B considered as a semiconductor InSb. In the terahertz (THz) frequency range (0.01-9.99 THz) and within the temperature range between 150 K and 360 K, the permittivity of semiconductor InSb can be described by the simple Drude model as: $\varepsilon_B(\omega) = \varepsilon_\infty - \omega_p^2/(\omega^2 + i\gamma\omega)$ and permeability $\mu_B = 1.0$, where ω is the angular frequency, ε_∞ (= 15.68) represents the static dielectric constant, γ is the damping constant, $\omega_p = \sqrt{Ne^2/\varepsilon_0 m^*}$ is a plasma frequency depends on the intrinsic carrier density *N*, the electronic charge e, the free space permittivity ε_0 and the effective mass m^* of the free carriers. The intrinsic carrier density *N* (in m^{-3}) of the semiconductor InSb depends on the temperature strongly and obeys the relationship; $N = 5.76 \times 10^{20} T^{3/2} \exp(-0.26/2k_B T)$, [Dai (2011); Li (2011)] where T is the temperature in Kelvin and k_B is the Boltzmann constant. The dependence of intrinsic carrier density *N*

on temperature makes the plasma frequency ω_p tunable by tuning the temperature. Consequently, refractive index of the semiconductor InSb $n_B(=\sqrt{\varepsilon_B.\mu_B})$ is very sensitive to temperature in the THz frequency range, which shows some anomalous and interesting optical characteristics in 1-D PCs consisting of semiconductor InSb. We can tune the refractive index of InSb by controlling external temperature T, which provides a method to achieve the tunable photonic and omnidirectional band gap in the PCs.

Table 5.1 Generations of the quasi-periodic sequences.

(i) Generation of the words $F_n = \sigma^n$ (A) of the Fibonacci sequence by the repeated action of the substitution rule σ (A) = AB, σ (B) = A.

Fibonacci Sequence	$F_{n+2} = F_{n+1}F_n$ with $F_0 = A$ and $F_1 = AB$	Number of Latters	Generation Number
F_0	A	1	0
F_1	AB	2	1
F_2	ABA	3	2
F_3	ABAAB	5	3
F_4	ABAABABA	8	4
…	……	…	…
…	……	…	so on.

(ii) Generation of the words $T_n = \sigma^n$ (A) of the Thue-Morse sequence by the repeated action of the substitution rule σ (A) = AB, σ (B) = BA.

Thue-Morse Sequence	$T_{n+1} = T_n \overline{T}_n$, $\overline{T}_{n+1} = \overline{T}_n T_n$, with $T_0 = A$ and $\overline{T}_0 = B$	Number of Latters	Generation Number
T_0	A	1	0
T_1	AB	2	1
T_2	ABBA	4	2
T_3	ABBABAAB	8	3
T_4	ABBABAABBAABABBA	16	4
…	……	…	…
…	……	…	so on.

(iii) Generation of the words $D_n = \sigma^n$ (A) of the Double-Periodic sequence by the repeated action of the substitution rule σ (A) = AB, σ (B) = AA.

Double-Periodic Sequence	$D_{n+1} = D_n \overline{D}_n$, $\overline{D}_{n+1} = \overline{D}_n D_n$, with $D_0 = A$ and $\overline{D}_0 = B$	Number of Latters	Generation Number
D_0	A	1	0
D_1	AB	2	1
D_2	ABAA	4	2
D_3	ABAAABAB	8	3
D_4	ABAAABABABAAABAA	16	4
…	……	…	…
…	……	…	so on.

To investigate the propagation of the electromagnetic wave in the quasi-periodic multilayer structures, we embrace the transfer matrix method to calculate the reflectance and band gap spectra. We assume that the electromagnetic wave is incident from the air to multilayer structures with incident angle θ. After applying the transfer matrix approach on the quasi-periodic multilayer structures, the electromagnetic wave propagation through the complete structures can be expressed by multiplying the characteristic matrices of the constituent layers (A and B). The amplitudes A_0 and B_0 of the electromagnetic field in the air medium at $x<0$ related to be the amplitudes A_{n+1} and B_{n+1} of the equivalent medium in the $(n+1)^{th}$ region through the linear transformation. Therefore, for the considered multilayer structures, the complete matrix expression can be written as; [Yeh (1988)]

$$\begin{pmatrix} A_0 \\ B_0 \end{pmatrix} = M_0^{-1}.(M_1.M_2.M_3 \dots M_n).M_0 \begin{pmatrix} A_{N+1} \\ 0 \end{pmatrix} \quad \dots\dots \quad \textbf{(5.1)}$$

where M_n is the 2×2 characteristic matrix of the n^{th} layer. These layers may be normal or graded materials or semiconductor materials. M_0 is the 2×2 characteristics matrix of air media. Finally, the transmittance (T) and reflectance (R) coefficients of the multilayer structures can be calculated as;

$$T = \left|1/M_{11}\right|^2 \text{ and } R = \left|M_{21}/M_{11}\right|^2 \quad \dots\dots \quad \textbf{(5.2)}$$

where M_{11} and M_{21} are the elements of the optical transfer matrix $M_{i,j}(i,j = 1,2)$ of the systems. For a period multilayer structure, based on Bloch's theorem and the boundary condition, the dispersion relation for a periodic multilayer system at any incident angle can be written as;

$$K(\beta,\omega) = \frac{1}{d}.cos^{-1}\left\{\frac{1}{2}(M_{11} + M_{22})\right\} \quad \dots\dots \quad \textbf{(5.3)}$$

where d is the total thickness of a period, M_{11} and M_{22} is the elements of the total characteristic matrix of a unit cell in the periodic multilayer structure. The dispersion relation exhibits multiple spectral bands classified into two regimes: First, where $|(M_{11} + M_{22})/2| \leq 1$ corresponds to real K and thus to propagating the Bloch waves. Second, spectral bands within which K is complex correspond to evanescent waves where $|(M_{11} + M_{22})/2| > 1$, that are rapidly attenuated and indicates the presence of band gaps, where the wave is inhibited that called photonic band gaps [Yeh (1988)].

5.3 Results and discussion

In this chapter, we have studied photonic band gap properties for different structural parameters, grading profile parameters, temperature and generations of Fibonacci, Thue-Morse and Double-periodic sequence in the quasi-periodic PC structures containing graded index materials and semiconductor. Our study has been carried out in the following parts.

5.3.1 Photonic band gap properties in 1-D quasi-periodic PC structures with graded index materials

In this section, we have first presented the reflection spectra and band gaps of the periodicity of second and third generations Fibonacci sequence. The unit cells of the considered structures are stacked of two types of layers namely A and B. Layers 'A' having constant refractive index equal to 1.5 and the other layers 'B' represent the graded index materials having refractive index variation from 1.5 to 4.1. In our calculations, the materials are considered as lossless dielectric, non-magnetic and their refractive index does not depend on frequencies. The reflectance spectra of the periodic structures $(F_2)^{10}$ and $(F_3)^{10}$ for different layer thicknesses and consisting of the layers of linear and exponential graded index materials having refractive index variation from 1.5 to 4.1, are shown in the figures 5.1(a and b) and 5.2 (a and b), respectively. The layers thicknesses of A and B are assume as $d_A = D/n_A$ and $d_B = D/n_B$, where D is considered as the layer thickness constant and relative refractive index of the layers are n_A and n_B, respectively. We consider the constant D = $\lambda_0/4$, $\lambda_0/2$, $3\lambda_0/4$ and λ_0, where λ_0 is the central wavelength of the incident wave and equal to 1000 nm. For second case, refractive index n_B is the mean value of initial and final refractive index of graded materials. Analysing the spectra shown in the figures 5.1(a and b) and 5.2(a and b), we observe that the number of reflection bands increases with the layers thickness. It is clear from these figures, number of reflection bands increases with increase of the integral multipliers of one-quarter of the optical wavelength (λ_0). In case of the structure with quarter-wave layer stacking arrangement, , the reflectance spectra show perfect reflection with broader bandwidth around the mid frequency range for the structure $(F_2)^{10}$ while perfect reflection regions are obtain towards lower and higher frequency ranges for the structure $(F_3)^{10}$. For the large layer thickness i.e. higher value of D, we get number of perfect reflection bands and their bandwidth become narrower and narrower as an indication of confinement of electromagnetic wave arising in different

frequency ranges. This property of such kind of structures gives rise to number of reflection bands, which may be useful to design filters for different regions. Moreover, the number of reflection bands also increases with increase of the generations of Fibonacci sequence in the periodic structures.

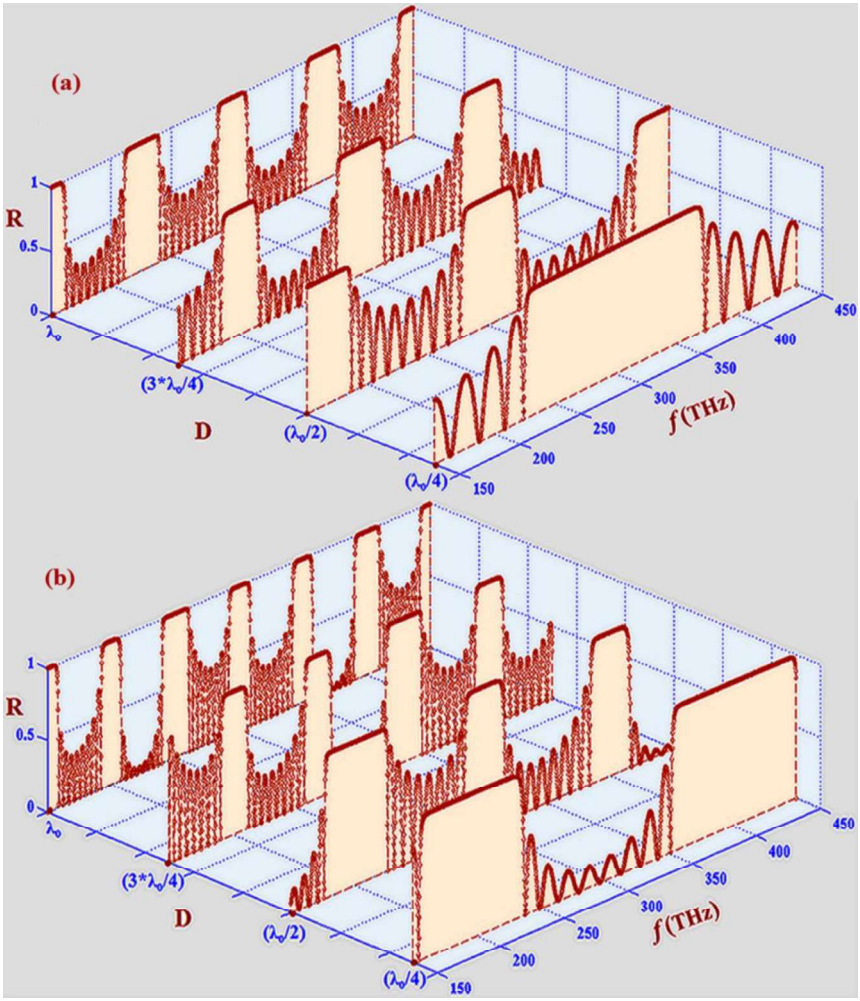

Figure 5.1 Reflection spectra calculated at different layer thickness constant (D) for the structures (a) $(F_2)^{10}$ and (b) $(F_3)^{10}$ with linear graded index material as one of the layer.

Due to the importance of the widespread and controlled PBGs in the periodic structures $(F_2)^{10}$ and $(F_3)^{10}$, we examine the confinement effects arising from competition between the structures induced by changing the thickness of layers and magnitude of the total stop bandwidth in the PBG spectra. To do that, we have calculate the regions for forbidden frequencies (stop bands), where $|(M_{11} + M_{22})/2| > 1$, as a function of the layers thickness and depicted in figure 5.3(a and) and 5.4(a and b) for the structures $(F_2)^{10}$ and $(F_3)^{10}$ with linear and exponential graded index material, respectively. These figures show the distribution of the forbidden (black region) and

allowed (white region) frequencies as a function of the layer thickness of the periodic structures $(F_2)^{10}$ and $(F_3)^{10}$ up to the value of $D = 7\lambda_0/4$.

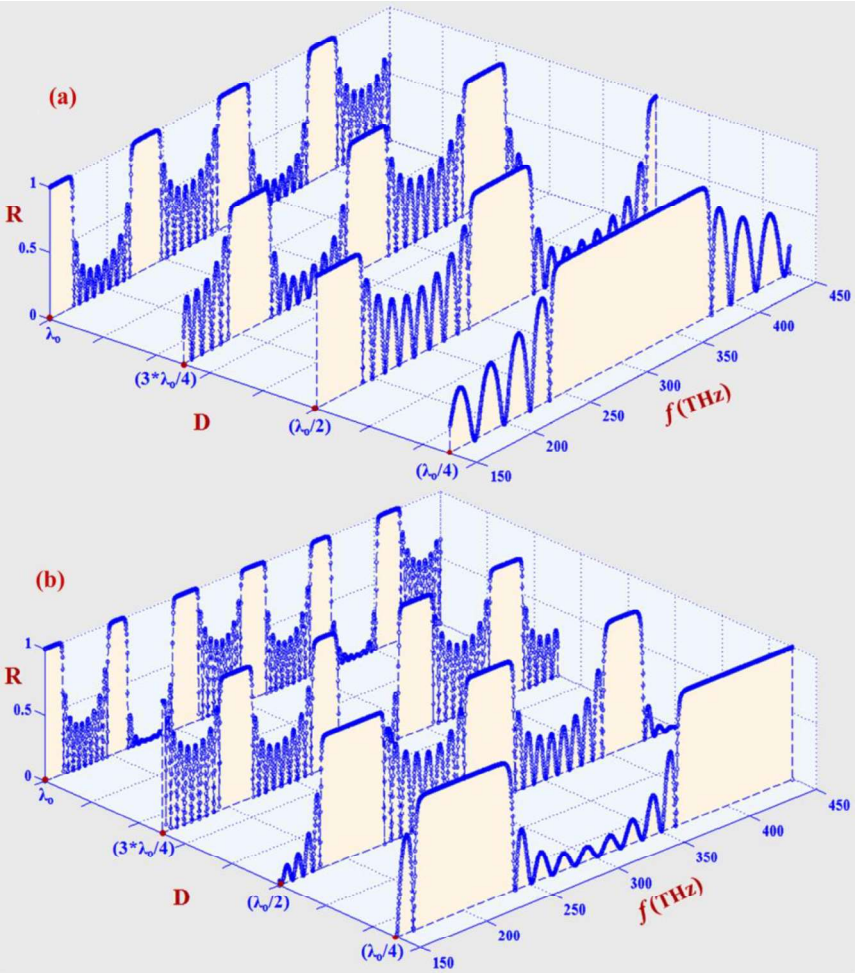

Figure 5.2 Reflection spectra calculated at different values of constant D for the structures (a) $(F_2)^{10}$ and (b) $(F_3)^{10}$ with exponential graded index material as one of the layer.

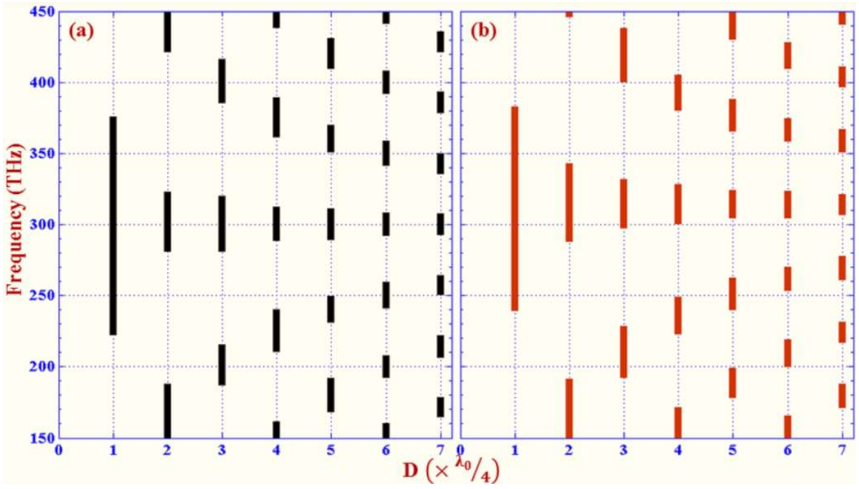

Figure 5.3 The distribution of PBGs as a function of layer thickness for the structure $(F_2)^{10}$ with (a) linear and (b) exponential graded index materials as one of the layer.

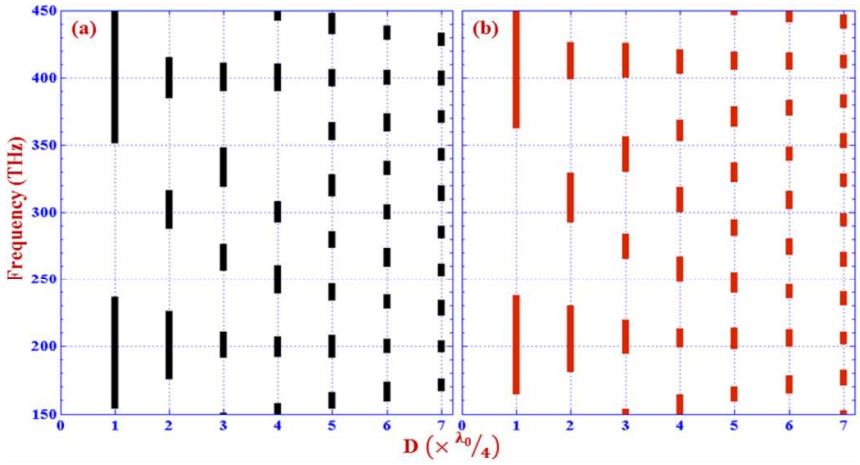

Figure 5. 4 The distribution of the PBGs as a function of layer thickness for the structure $(F_3)^{10}$ with (a) linear and (b) exponential graded index material as one of the layer.

Note that, as expected, for large layer thickness, we get number of forbidden bands and their bandwidth become narrower and narrower as an indication of more PBGs with small bandwidth. The variation of forbidden bands with the layer thickness of for the structures $(F_2)^{10}$ and $(F_3)^{10}$ with linear and exponential graded index material are clearly depicted in the figure 5.3 and 5.4, respectively. Moreover, we have shown the total band gap verses the layer thickness for the structures $(F_2)^{10}$ and $(F_3)^{10}$ in figure 5.5. It reveals that the total band gap randomly decreases with increasing the layer thickness, but total photonic band gap is extremum for the quarter-wave stacked arrangements in all cases.

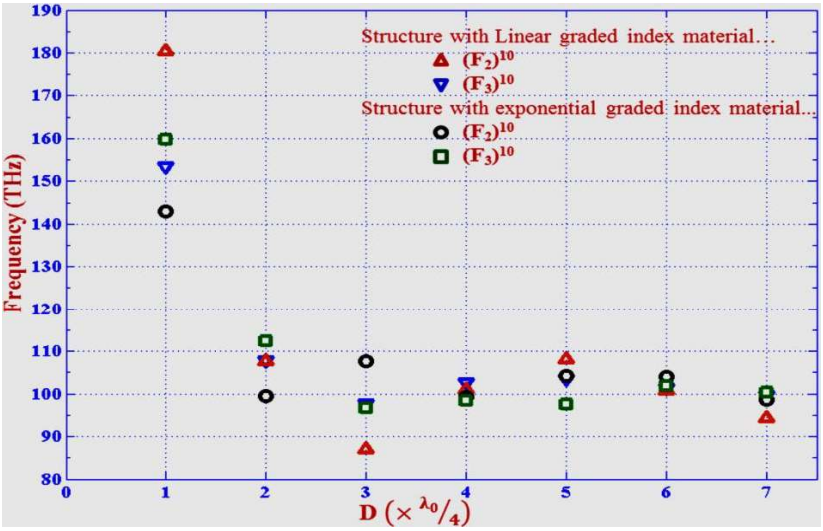

Figure 5.5 The variations of total bandwidth as a function of the layer thickness for the structure $(F_2)^{10}$ and $(F_3)^{10}$ with (a) linear and (b) exponential graded index materials as one of the layers.

To see the effect of grading, we have calculated the reflectance spectra of the

structures $(F_2)^{10}$ and $(F_3)^{10}$ with quarter-wave stacked arrangements for different values of grading profile parameter of linear (α) and exponential (γ) graded layer. Reflectance verses frequency curves are shown in the figures 5.6(a and b) and 5.7(a and b) for the structures $(F_2)^{10}$ and $(F_3)^{10}$ with linear and exponential graded index materials, respectively. We observe that the reflectance spectra for $(F_2)^{10}$ and $(F_3)^{10}$ are contradictory in nature. In case of the $(F_2)^{10}$, the obtained reflectance spectra show perfect reflection for the mid frequency range, while for the structure $(F_3)^{10}$, perfect reflection regions are exist towards lower and higher frequency ranges. The reflection band gaps region increases as increasing the value of grading profile parameter α (γ) of the linear (exponential) graded layer. Because, the change in grading profile parameters ultimately provides the enhancement in contrast of the refractive index among the layers. The reflection bands of the relative structures are exist at the higher frequency region for exponential graded index material as compared to the linear graded index material as one of the layer in the considered structures.

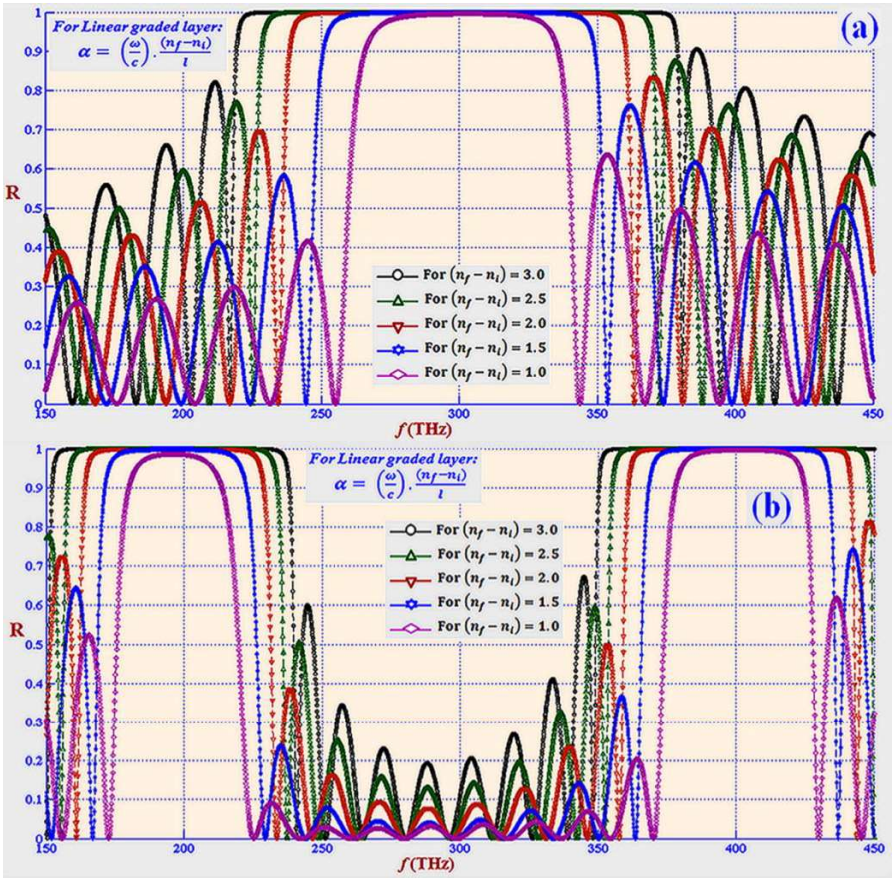

Figure 5.6 Panels (a) and (b) show the reflectance spectra at different values of grading profile parameter 'α' of linearly graded index material layers in the structures $(F_2)^{10}$ and $(F_3)^{10}$, respectively.

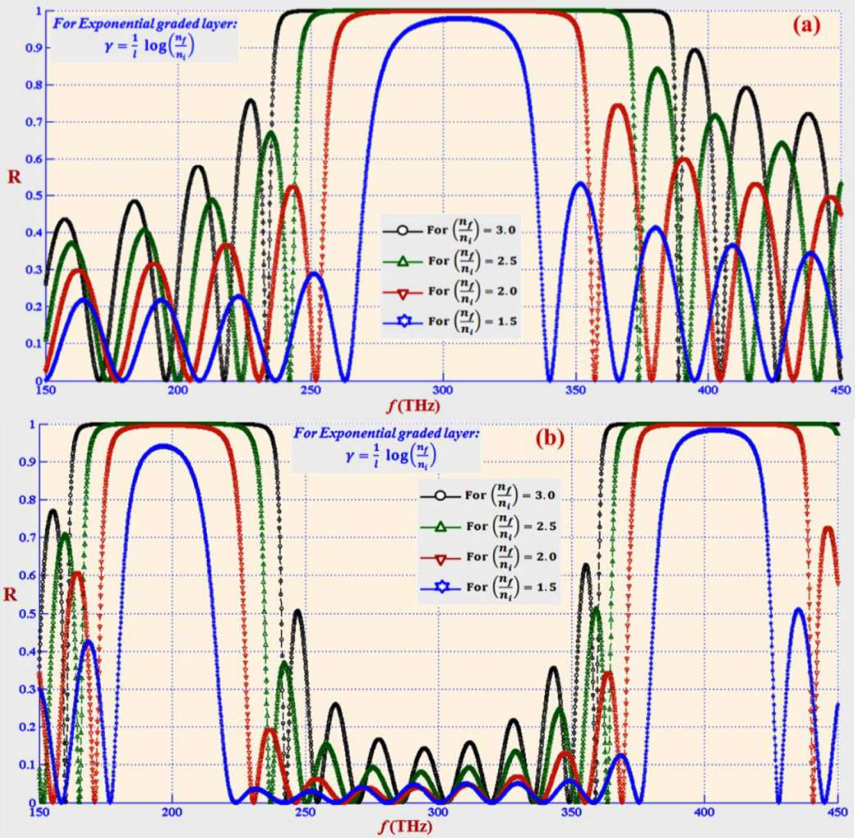

Figure 5.7 Panels (a) and (b) show the reflectance spectra at different values of grading profile parameter 'γ' of exponentially graded index layers in structures $(F_2)^{10}$ and $(F_3)^{10}$, respectively.

The investigation clearly demonstrate that the thicknesses and grading profiles parameters of graded index materials layers have great influence on the photonic band gaps, and structures with periodicity of different generation Fibonacci sequence have some promising applications because they confine light in a new way by different structural scattering. Therefore, we can obtain the suitable PBGs by adjusting the layer thickness and gradation profile parameters and changing by the generations of Fibonacci sequence in the proposed structures.

Now, we investigate the influence of higher order Fibonacci sequence on the reflection spectra and localization modes for linear and exponential graded index material as one of the layer in the considered quasi-periodic structures such as F_7, F_8 and F_9 structures, where F_n represents the n^{th} generation Fibonacci sequence. The optical reflection spectra of the considered 1-D quasi-periodic structures arranged in Fibonacci sequence F_7, F_8 and F_9 for normal material, linear and exponential graded index materials in the frequency range of 150 - 450 THz are shown in figures 5.8(a), 5.8(b) and 5.8(c), respectively. Analysing these spectra, we find that the reflection spectra is

symmetric and the one central dip in F_7, F_8 and F_9 is always at the middle value of considered frequency range i.e. 300 THz when the B layer is of constant refractive index. The number of localization mode and their intensity in these structures are changed with the increase of Fibonacci generation. This happened because the number of layers increases as increase the order of Fibonacci generation.

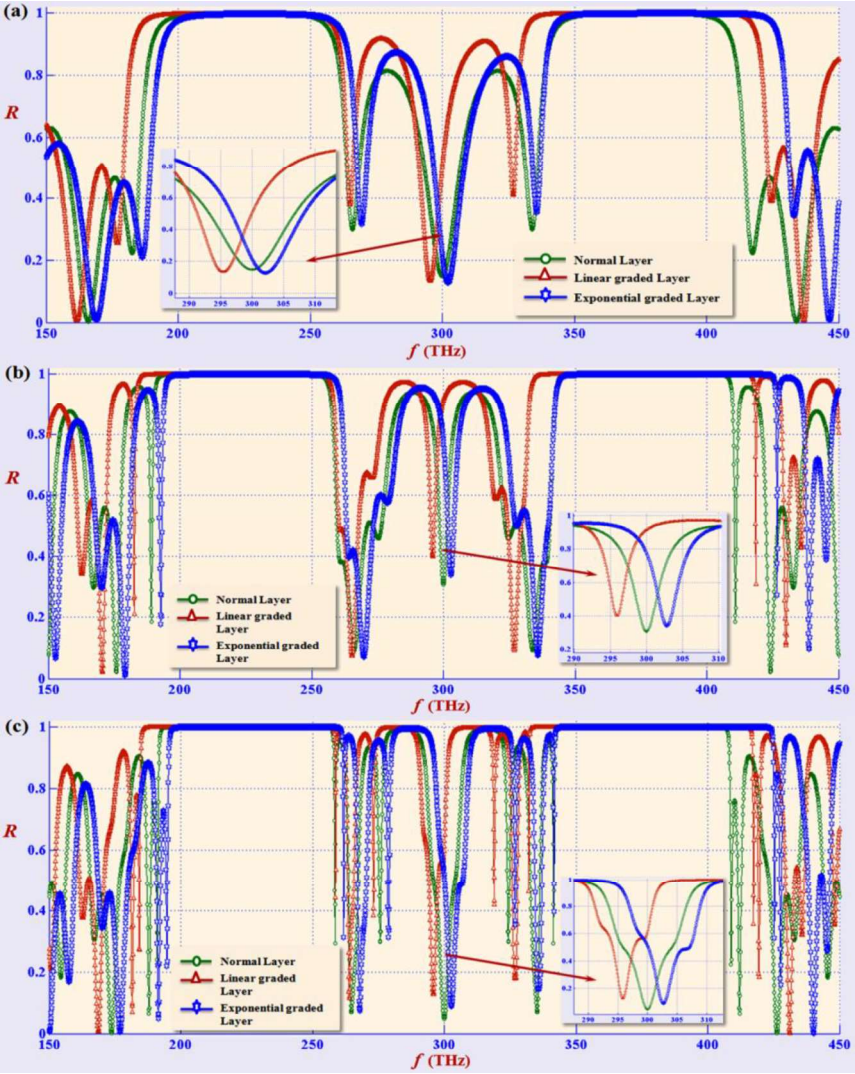

Figure 5.8 Reflectance (R) versus frequency (*f*) spectra of the structures (a) F_7, (b) F_8 and (c) F_9 for normal, linear and exponential graded index materials under normal incidence.

Considering B type layers of linear graded material, we find that the reflection band gaps increases and shifted towards the lower frequency side whereas when B type layer is of exponentially graded material, the reflection band gap also increases but shifted towards the higher frequency side. The central dip in all F_7, F_8 and F_9 structures is also shifted towards the lower and higher frequency side for considering B type layers of linear and exponential graded materials respectively, but shifted position is always at

the approximate same value of frequency for all structures. Form these spectra we observe that the grading profiles are able to shift the localization modes. The shifting of localization modes and increasing reflection band gap would be able to recognize the grading profile of the materials used in 1-D Fibonacci quasi-periodic structures.

Now, we present the reflection spectra of light and PBG properties for different 1-D quasi-periodic (Thue-Morse and Double-Periodic) type multilayer structures. The unit cells of considered 1-D quasi-periodic photonic structures are stacked of two types of layers namely A and B, where 'A' type layers represent constant refractive index (Normal) material of value 1.5 and 'B' type layers represent linear and exponential graded index material having refractive index variation from 1.5 to 4.5. We have calculated the reflectance and band spectrum of light incident normally through the air on the considered multilayer structures.

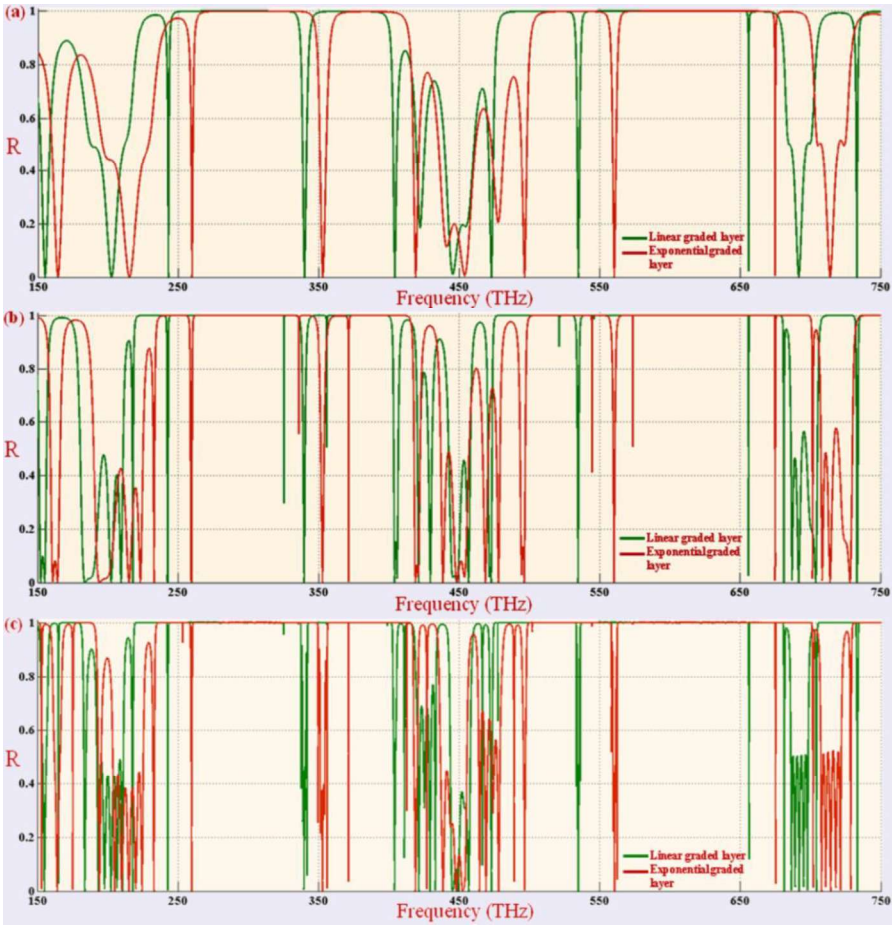

Figure 5.9 Reflection coefficient (R) versus frequency for the quasi-periodic photonic crystal structures of (a) 5th, (b) 6th and (c) 7th generation Thue-Morse sequence with linear and exponential graded materials.

We first present the reflection spectra of 1-D Thue-Morse quasi-periodic photonic

structures for Fifth, sixth and seventh generation with linear and exponential graded index materials as layer B. Thickness of the layer A and B are chosen in terms of quarter wave stacking i.e. $n_A d_A = n_m d_B = \lambda_0/4$, where d_A and d_B are the thickness of layer A and B respectively, and n_m is the mean value of initial refractive index and final refractive index of the graded layer. The parameters are $n_A = 1.5$, $n_m = 3.0$ and wavelength λ_0 is the mean value of the considered frequency region (150 - 750 THz). Analysing results are shown in figure 5.9. The number of localization modes and forbidden bands are observed and which are increases with increasing the generation of Thue-Morse sequences. It is clearly visible that localization modes and forbidden bands exist in higher frequency region for the structures with exponential graded material as compare to the structures with linear graded material. The influence of different graded materials on the localization modes and band gaps are sighted on position and width of band gaps whereas numbers of localization modes and forbidden bands are same.

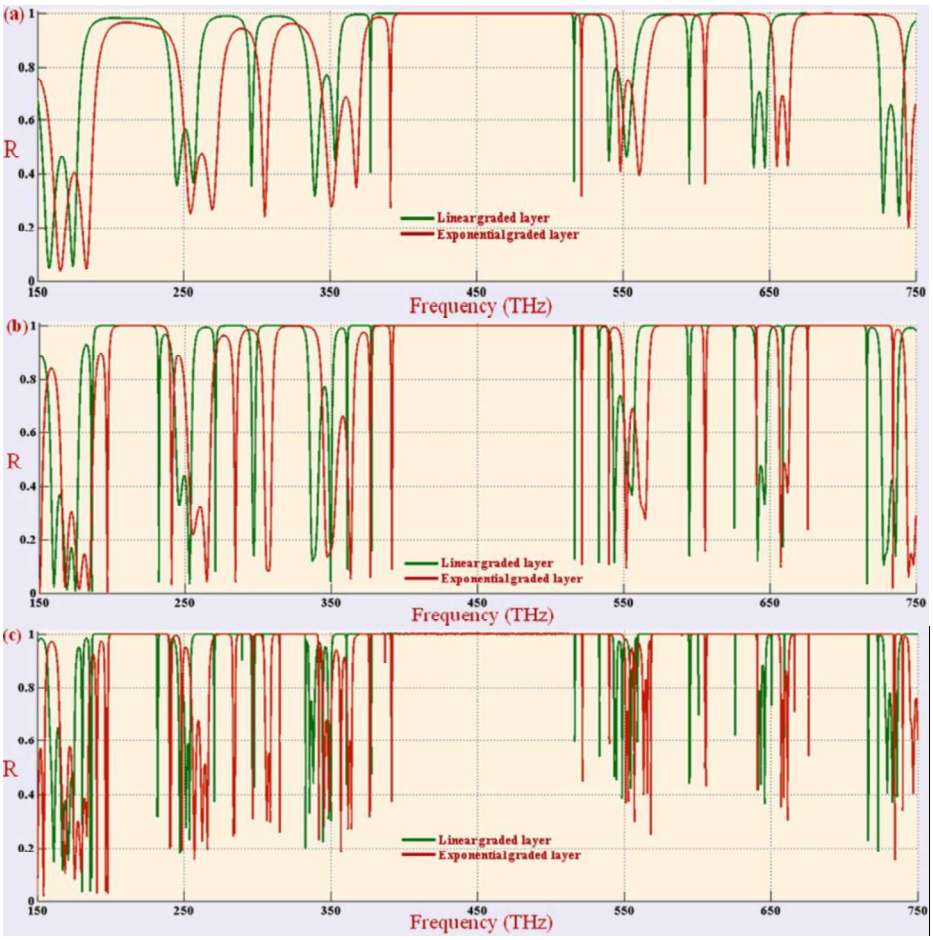

Figure 5.10 Reflectance (R) versus frequency for the structures of (a) 5th, (b) 6th and (c) 7th generation Double-Periodic sequence with linear and exponential graded materials.

Likewise, we have studied the influence of graded index materials on the localization modes and forbidden bands for 1-D Double-Periodic photonic structures for Fifth, sixth and seventh generation with linear and exponential graded index material under normal incident of light. In these structures, composition of the layer arrangement are different, but other parameters such as thickness, total number of layer in the structures are same with respect to same generation of Thue-Morse quasi-periodic structures. Reflection spectra of these structures are shown in figure 5.10. The numbers of localization modes and forbidden band increases with the increase of the generation of Double-Periodic quasi-periodic system, and the shifting of localization modes and forbidden bands are similar as the case of 1-D Thue-Morse quasi-periodic structures. One broader forbidden band always exists at the central frequency region for the Double-Periodic quasi-periodic system, while bands exist at lower and higher frequency region for the structures with Thue-Morse quasi-periodic structures. Figures 5.9 and 5.10 clearly demonstrated the number and position of localization mode and forbidden band depends on the generation of quasi-periodic systems. The results also show the position of modes and bands exist at higher frequency for structures with exponential graded material as compare to the structures with linear graded materials, because the rate of change of refractive index contrast in exponential graded material layer slightly high in comparison to the linear graded material layer. On the other hand, initial and final refractive indices are same in both type of graded materials layer and hence the change in initial to final optical path length is approximate same, therefore due to this fact, structures have equivalent number of modes and bands.

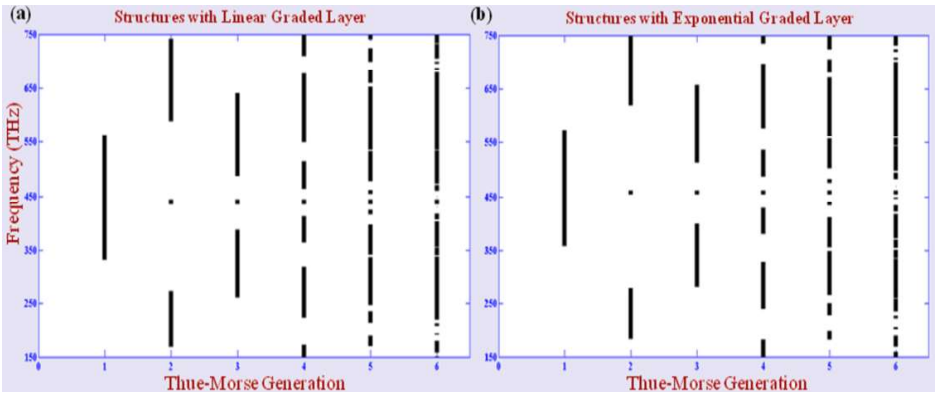

Figure 5.11 The distribution of the photonic bandwidths as a function of the Thue-Morse generations for the structures with (a) linear and (b) exponential graded layers.

Furthermore, we have examined the photonic band gap spectrum of the periodic super lattice of different quasi-periodic (Thue-Morse and Double-Periodic) generations

arising from competition between the linear and exponential graded layer, and depicted in panels (a) and (b) of the figures 5.11 and 5.12, respectively. For this analysis, we have calculated the forbidden frequencies (stop bands), where $|(M_{11} + M_{22})/2| > 1$, as a function of the generation of the quasi-periodic (Thue-Morse and Double-Periodic) sequence for a fixed value of $n_m d_B = \lambda_0/4$, and shown in the figure 5.11 (Thue-Morse sequence), and figure 5.12 (Double-Periodic sequence).

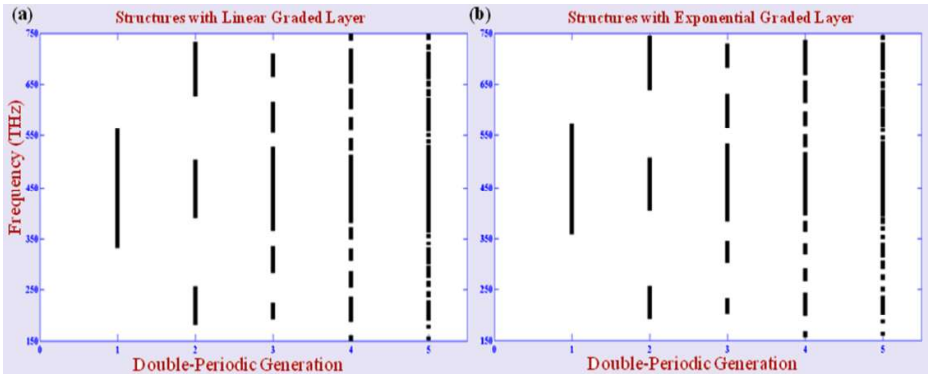

Figure 5.12 The distribution of the photonic bandwidths as a function of the Double-Periodic generations for the photonic crystal structures with (a) linear and (b) exponential graded layers.

Figure 5.11(a) and 5.11(b) show the distribution of the forbidden (black region) and allowed (white region) frequencies as a function of the generation of the Thue-Morse sequence up to the 6th generation for the structures with linear and exponential graded materials layer, respectively. As expected, for large number of generations, we get large number of stop bands and their bandwidth become narrower and narrower as an indication of more localized modes. We also observed that number of band gap in the structures with both linear and exponential graded materials layer presents a similar distribution as a function of the generation of the Thue-Morse sequence, but their bandwidth and frequency region are slightly different. Likewise, the distribution of the bandwidths for the Double-Periodic structures up to the fifth generation of the sequence with linear and exponential graded material layer has been described in figures 5.12(a) and 5.12(b), respectively. A similar behaviour like the Thue-Morse case is obtained but bandwidth and band region of PBG are slightly different. The number of band gap in these structures with linear and exponential graded material layer increases with generation of the Double-Periodic sequence. The frequency regions of the stop bands exist at higher frequency point for structures with exponential graded layer as compare to the structures with linear graded layer, but bandwidths in case of linear graded layer are slightly large. This fact is clearly demonstrated in the figures 5.11 and 5.12.

Finally, the distribution of the total bandwidth variation as a function of the generation of the Thue-Morse and Double-Periodic sequence for the quasi-periodic structures with linear and exponential graded materials layers is described in the figures 5.13(a) and 5.13(b), respectively. These figures show that the total bandwidth of the forbidden energy regions increases with the generation of the Thue-Morse and Double-Periodic sequences for the structures with linear and exponential graded materials layers, but the total bandwidths are high for the Thue-Morse and Double-Periodic structures with linear graded material layers as compare to the structures with exponential graded material layers for each generation level. In case of the Double-Periodic structures, the variation of total bandwidths is in a linear way with generation of sequence, while in case of the Thue-Morse structures variations are not in linear way, and the values of the total bandwidths are high for the Double-Periodic structures with both types of graded materials layers in comparison to the Thue-Morse structures. These investigations clearly demonstrate the influence of linear and exponential graded index materials on the existence of localization modes, photonic bandwidth and their band region in the Thue-Morse and Double-Periodic multilayer structures.

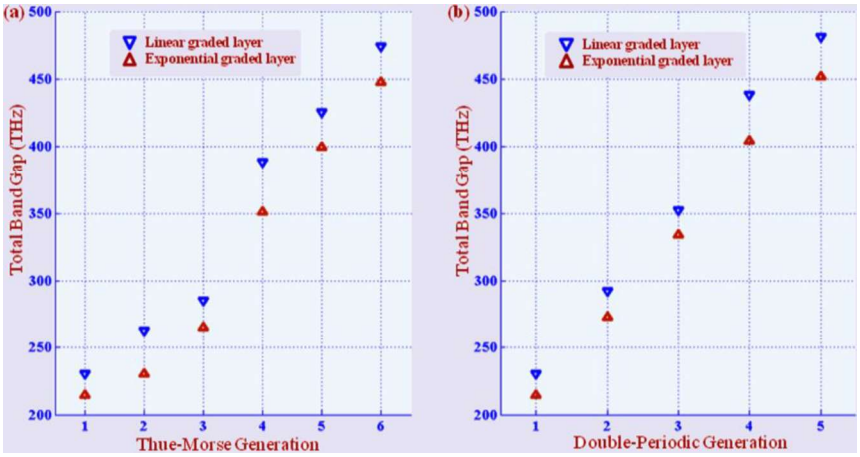

Figure 5. 13 The total band gap variation with the generations of the sequence (a) Thue-Morse and (b) Double-Periodic in photonic crystal structures with linear and exponential graded layers.

5.3.2 Photonic band gap properties in 1-D quasi-periodic photonic crystals with semiconductor

In this section, the numerical results to characterize the optical reflection, photonic and Omni-directional band structures at different temperature and structural parameters in 1-D quasi-periodic (Fibonacci, Thue-Morse and Double-Periodic) PC structures have presented. The unit cells of the considered 1-D quasi-periodic PC

structures are stacked of two types of medium A and B. We consider the medium A as dielectric material (SiO_2) with $\varepsilon_A = 2.25$ and $\mu_A = 1$, while medium B as semiconductor (InSb) with $\mu_B = 1$ and $\varepsilon_B(\omega)$, which are given in theoretical description section and assuming $\gamma = 0$, $\varepsilon_\infty = 15.68$, $m^* = 0.015m_e$ and $m_e = 9\times10^{-31}$ kg. In this study, we also assume that light incident through the air medium and losses of the dielectric and semiconductor material are neglected. The considered quasi-periodic multilayer structures using layer A and B are obtained according to the substitution rules of the Fibonacci, Thue-Morse and Double-Periodic sequences, which are listed in table 5.1.

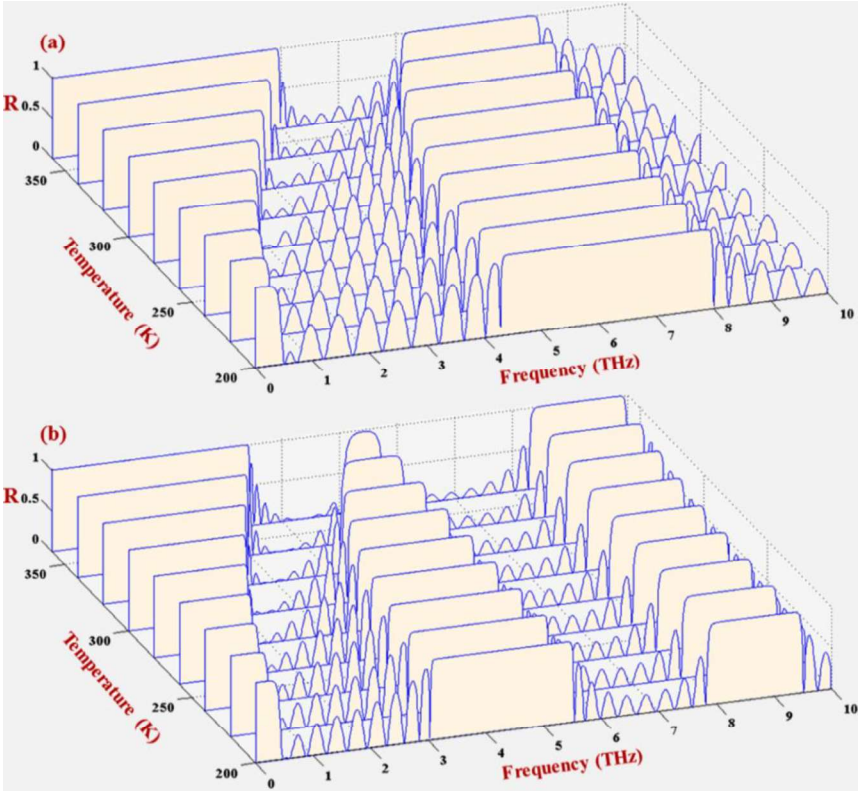

Figure 5.14 Reflectance (R) of the structure (a) $(F_2)^{10}$ and (b) $(F_3)^{10}$ as a function of frequency with varying temperature, and assuming $d_1 = 7$ μm and $d_2 = 3.5$ μm.

First, we present the reflection spectra, photonic and omnidirectional band gap characteristic of 1-D Fibonacci quasi-periodic photonic structures at different temperature and layer thickness in THz region (0.01-9.99 THz). The reflection spectra of the structure $(F_2)^{10}$ and $(F_3)^{10}$ for different temperature under normal incidence are shown in the figures 5.14(a) and 5.14(b). We assumed that d_1=7.0 μm and d_3=3.5 μm, and F_n represents n^{th} order Fibonacci sequence. From these figures, one sees that the upper band-edge of gap I shift to higher frequency and their bandwidth becomes broader as increases of temperature, which is resulted from the change of dielectric

function of the semiconductor material InSb with temperature. However, both lower and upper band-edges of higher order band gaps of the structures $(F_2)^{10}$ and $(F_3)^{10}$ shift toward higher frequency and bandwidths become narrow and narrow as increasing the temperature. We can also see clearly that one new photonic band gaps is appear in the structure $(F_3)^{10}$ for same lattice constant. The remarkable modification in photonic band gaps offers an approach to realize thermally tunable photonic devices in THz region.

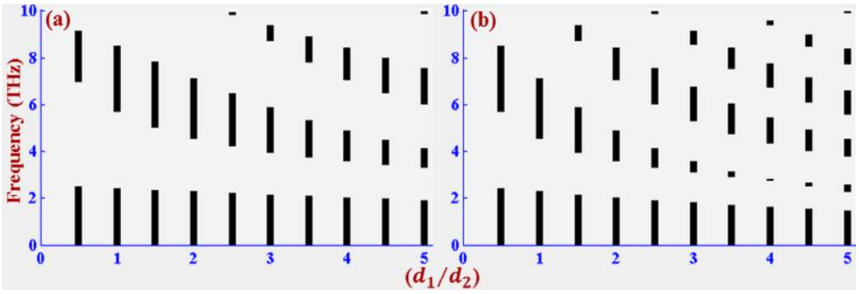

Figure 5.15 The distribution of the photonic band gaps as a function of the thickness ratio (d_1/d_2) at normal incidence for the structure (a) $(F_2)^{10}$ and (b) $(F_3)^{10}$, where $d_2 = 4$ μm and T = 300 K.

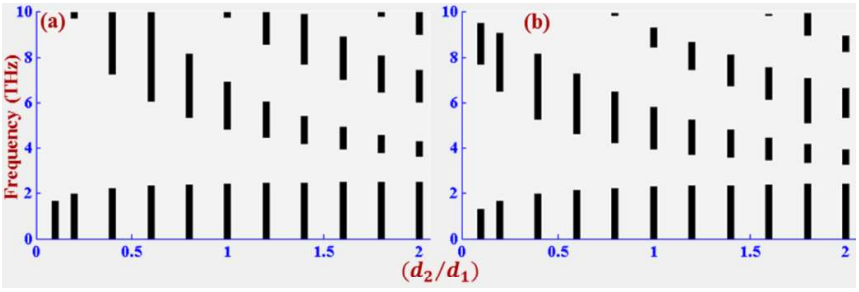

Figure 5.16 The distribution of the photonic band gaps in the structure (a) $(F_2)^{10}$ and (b) $(F_3)^{10}$ as a function of the thickness ratio (d_2/d_1) at normal incidence, where $d_1 = 5$ μm and T = 300 K.

To examine the confinement effects arising from competition between the structures induced by changing the thickness of layers and magnitude of the photonic bandwidths in PBG spectra. To do that, we have calculate the regions for forbidden frequencies (stop bands) as a function of the thickness of layers for the structure $(F_2)^{10}$ and $(F_3)^{10}$. The dependence of PBGs on the thickness ratio (d_1/d_2) with fix the thickness $d_2 = 4.0$ μm and thickness ratio (d_2/d_1) with fix the thickness $d_1 = 5.0$ μm are shown in figures 5.15 and 5.16, respectively. These figures show the distribution of forbidden (black region) and allowed (white region) frequencies as a function of the layer thickness ratio for the structures $(F_2)^{10}$ and $(F_3)^{10}$ in the panel (a) and (b) of the figure 5.15 and 5.16, respectively. It is clearly seen that more and more PBGs appear as the increase of the thickness ratio. In figure 5.15, the upper band-edge of first gap shifts to

lower frequency as increasing the thickness ratio (d_1/d_2) with $d_2 = 4.0$ μm, but the lower band edges are unchanged. However, both the upper and lower band-edges of the higher order band gaps shift to lower frequency and bandwidth of these gaps becomes more and more narrow as increasing the thickness ratio (d_1/d_2). In the case of figure 5.16, the upper band-edge of the first gap shifts toward higher frequency as increasing the thickness ratio (d_2/d_1) with $d_1 = 5.0$ μm, but the lower band edges are unchanged. However, the characteristics of higher order band gaps are approximately similar as in the case of figure 5.15. Particularly, the bandwidth of higher order band gaps in both cases becomes narrower with the increase of layer thickness ratio. It is found that the frequency position and bandwidth of the photonic band gaps is controllable by adjusting the thickness of medium. The change in thickness of the semiconductor layers is more effective on the photonic band gaps uue to changing of dielectric function with frequency, which provides us a scheme to realized tunable PBGs in the structures. Therefore, such type structures can be used as multi-channel filters by adjusting the layer thicknesses.

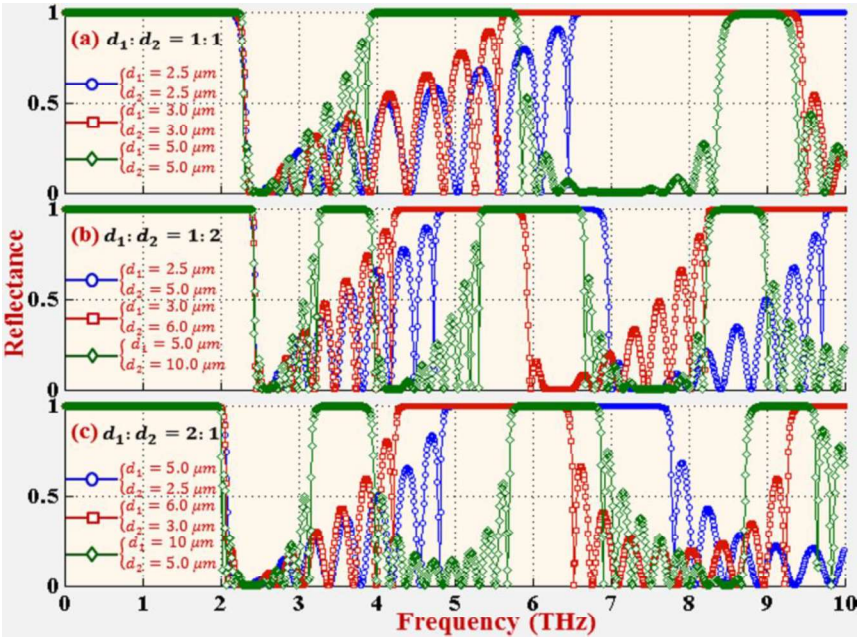

Figure 5.17 Reflectance (R) spectra of the structure $(F_2)^{10}$ at normal incidence under different fixed layer thickness ratio (a) $d_1:d_2 = 1:1$, (b) $d_1:d_2 = 1:2$ and (c) $d_1:d_2 = 2:1$, and T = 300 K.

Due to importance of the tunable PBGs, we have checked the influence of constant thickness ratio on the PBG and illustrated in figure 5.17 at different fixed layer thickness ratios. We assume three different cases of constant layer thickness ratio (a) $d_1:d_2 = 1:1$ with layers thickness (i) $d_1 = 2.5$ μm and $d_2 = 2.5$ μm, (ii) $d_1 = 3.0$ μm and d_2

= 3.0 μm, (iii) d_1 = 5.0 μm and d_2 = 5.0 μm, (b) d_1:d_2 = 1:2 with layers thickness (i) d_1 = 2.5 μm and d_2 = 5.0 μm, (ii) d_1 = 3.0 μm and d_2 = 6.0 μm, (iii) d_1 = 5.0 μm and d_2 = 10.0 μm, and (c) d_1:d_2 = 2:1 with layers thickness (i) d_1 = 5.0 μm and d_2 = 2.5 μm, (ii) d_1 = 6.0 μm and d_2 = 3.0 μm, (iii) d_1 = 10.0 μm and d_2 = 5.0 μm. From figure 5.17, we can clearly see that the first band gap in all cases is invariant, the edges and bandwidth of this PBG are staying the same as increasing the layer thickness with fixed thickness ratio d_1/d_2. However, the higher order PBGs is sensitive to the lattice parameters. The edges of the higher order PBGs shift to lower frequency and bandwidth of these bands become more and more narrow. It can also clearly see that more and more PBGs appear within same frequency range as the increase of lattice parameter. Moreover, bandwidth of the first PBG decreases as increasing the thickness ratio (d_1/d_2).

To take a look at the confinement effects arising from competition between the long-range aperiodic orders induced by the Fibonacci quasi-periodic structures, we have calculated the forbidden frequencies (stop bands) as a function of the generation of the Fibonacci sequence. In figure 5.18, we have demonstrated the distribution of the bandwidths of the forbidden (black region) and allowed (white region) frequencies as a function of the Fibonacci generation up to 7^{th} generation under normal incidence and lattice constant d_1 = 7 μm and d_2 = 3 μm, and temperature T = 300 K. We get number of forbidden bands and their bandwidth becomes narrower and narrower as the increase of the Fibonacci generation and also get more localized modes.

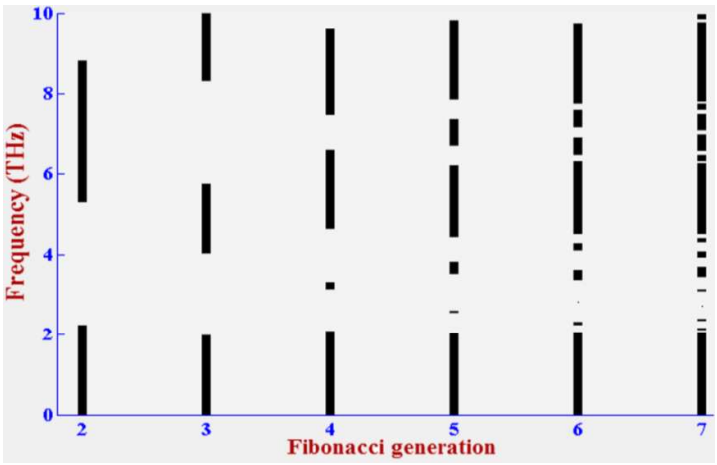

Figure 5.18 The distribution of the photonic bands as a function of the Fibonacci generation in the 1-D Fibonacci multilayer structures with lattice parameters d_1 = 7 μm, d_2 = 3 μm and temperature T = 300 K.

To discuss the OBG characteristics in the Fibonacci quasi-periodic structures $(F_2)^{10}$ and $(F_3)^{10}$, we have shown the reflectance spectra at different incident angle up to

89^{o} for TE and TM polarization in the figures 5.19(a and b) and 5.20(a and b), and the projection band structures as changing of the incident angle exhibited in figure 5.19(c) and 5.20(c), respectively. We assume lattice constant d_1 = 7 μm and d_2 = 3 μm, and temperature T = 300 K. These figures clearly demonstrate the distribution of the PBGs as changing of the incident angles in the structures $(F_2)^{10}$ and $(F_3)^{10}$. There are the OBGs that exist between higher and lower band edges as prevalent band region for both TE and TM polarization.

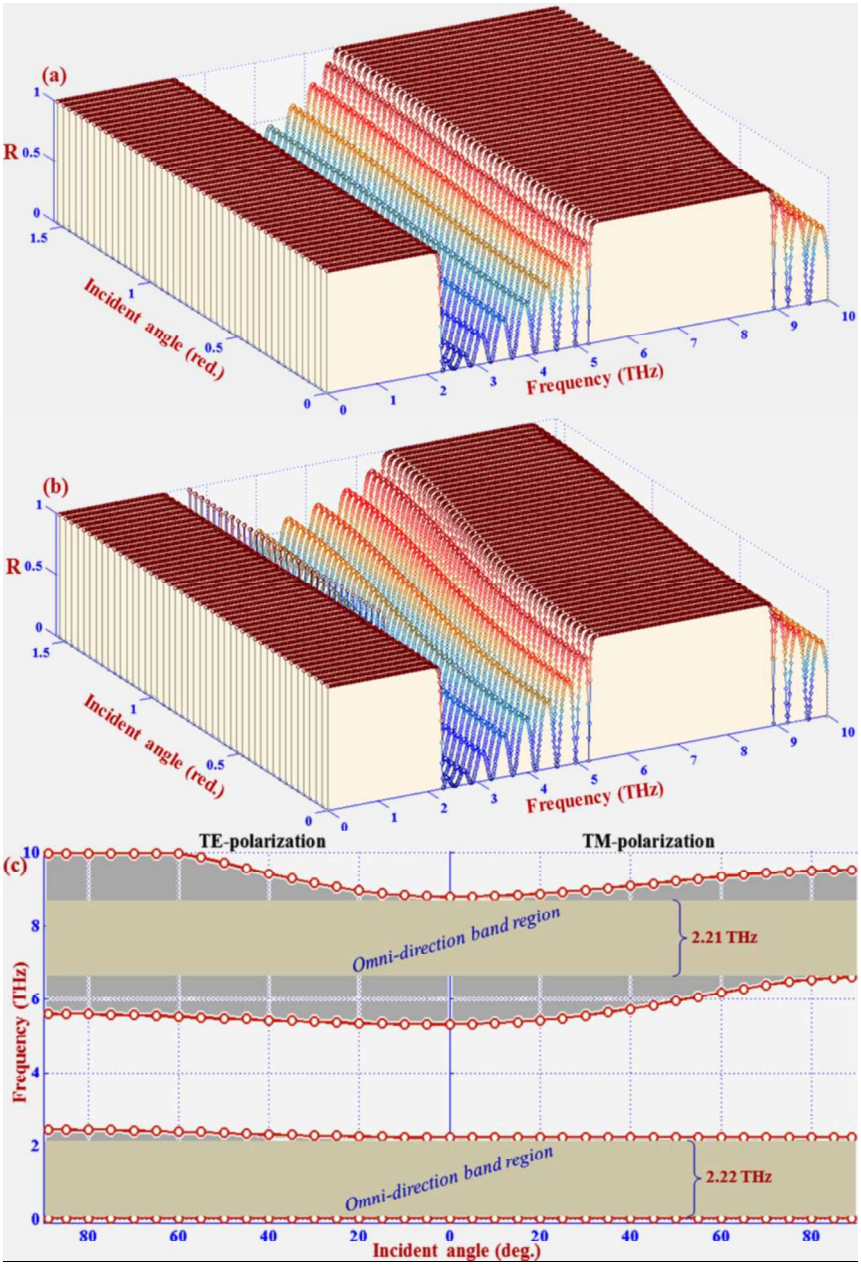

Figure 5.19 Reflectance (R) spectra for (a) TE-polarization, (b) TM-polarization and (c) projected band gaps structure as a function of incident angle in the structure $(F_2)^{10}$ with lattice parameters d_1 = 7 μm, d_2 = 3 μm and temperature T = 300 K.

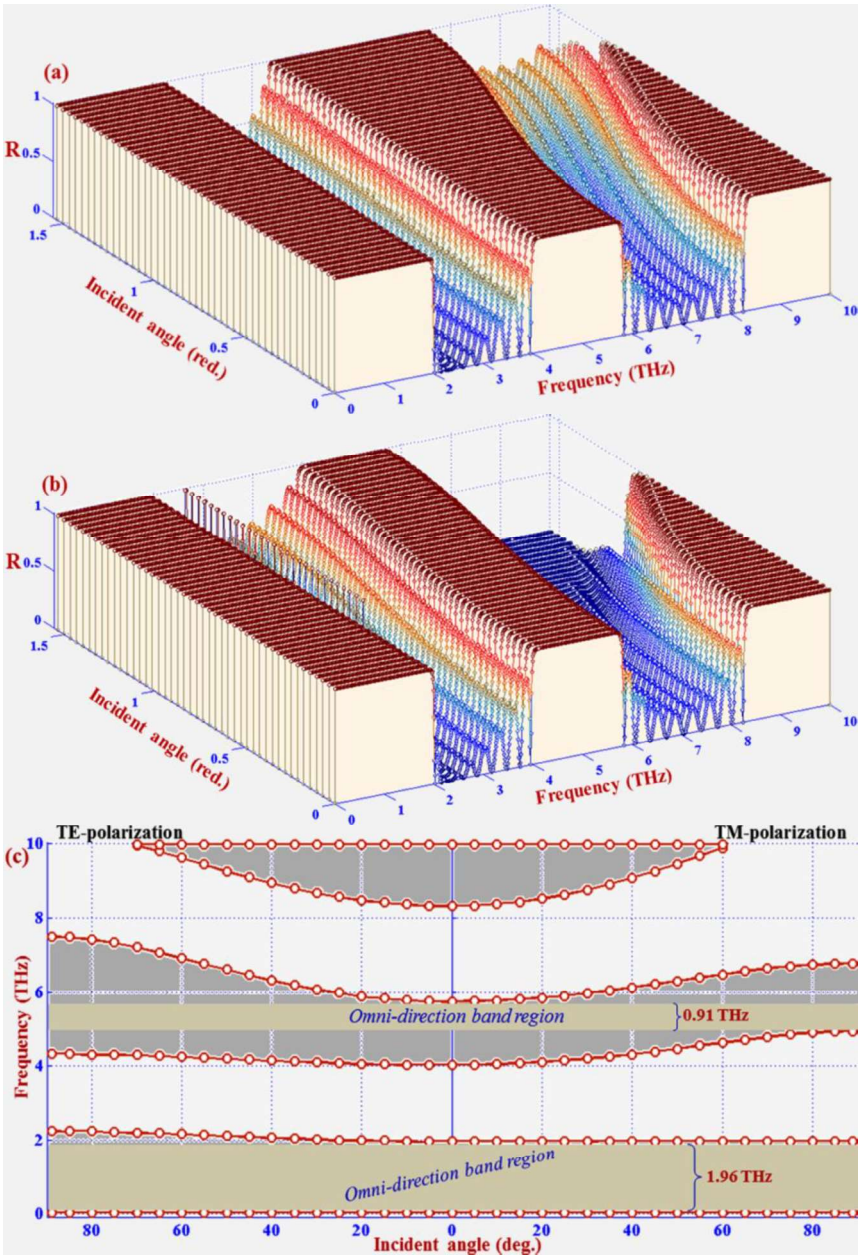

Figure 5.20 Reflectance (R) spectra of the structure $(F_3)^{10}$ for (a) TE-polarization, (b) TM-polarization and (c) projected band gaps structure as a function of incident angle, and assuming lattice parameters $d_1 = 7$ μm, $d_2 = 3$ μm and temperature T = 300 K.

In figures 5.19(c) and 5.20(c), the gray areas represent the forbidden band gaps and the ubiquitous white area between the higher and lower band edges of PBG in both polarizations illustrates the OBGs. There exist two OBGs in both structures $(F_2)^{10}$ and $(F_3)^{10}$. The omnidirectional bandwidths are 2.22 THz and 2.21 THz for the structure $(F_2)^{10}$, and 1.96 THz and 0.91 THz for the structure $(F_2)^{10}$. Furthermore, to investigate the effects of temperature on the OBGs, we have shown the distribution of OBGs as the change of temperature in the figures 5.21(a) and 5.21(b) for the structures $(F_2)^{10}$ and

$(F_3)^{10}$, respectively. From these figures, we can see that the bandwidth of first order OBGs increases while the bandwidth of second order OBGs decreases as increasing the temperature. Because the dielectric constant of the semiconductor InSb depends on the temperature strongly that provides tunable PBGs. The edges of the second order OBGs move to higher frequency. The change in bandwidth of first order OBGs is more sensitive to the second order OBGs as the change of temperature.

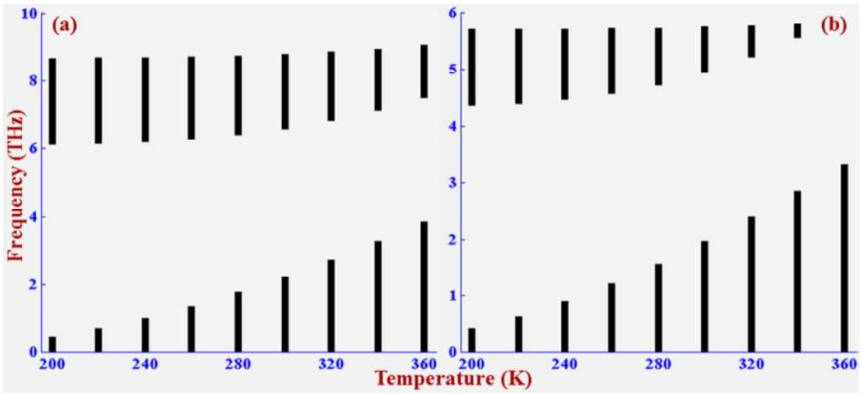

Figure 5.21 Distribution of the omnidirectional band gaps as a function of temperature for the structures (a) $(F_2)^{10}$ and (b) $(F_3)^{10}$, here lattice parameters $d_1 = 7$ μm and $d_2 = 3$ μm.

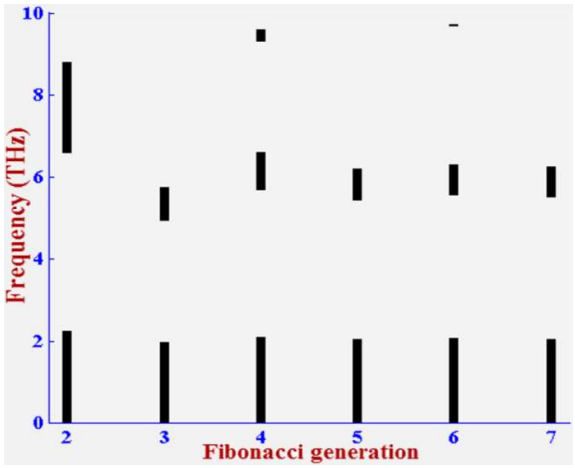

Figure 5.22 The distribution of the omnidirectional bands as a function of Fibonacci generation of the structures with lattice parameters $d_1 = 7$ μm, $d_2 = 3$ μm, and T = 300 K.

In order to discuss the effect of Fibonacci generation on the OBGs, we have plotted the OBGs versus Fibonacci generation in the figure 5.22 and assuming parameters are $d_1 = 7$ μm, $d_2 = 3$ μm and T = 300 K. We can see that the higher band edges of the first order OBGs slightly change the frequency limits while the lower band edges are invariant, and their bandwidth having very small changes, when changing the generations of Fibonacci sequence. However, the upper and lower frequency limits of the second order OBGs randomly change the frequency and the bandwidth of this band

gaps also changes as increasing the Fibonacci generation. In the case of fourth and sixth order Fibonacci generation, we get third order OBGs with very small bandwidths.

The above evaluation shows that the photonic and omnidirectional band gaps can be achieved in 1-D Fibonacci multilayer structures composed of the semiconductor material InSb and dielectric material SiO_2. The position and bandwidth of the photonic and omnidirectional band gaps can be tuned through the change of the external temperature, lattice parameters and generation of the Fibonacci sequences.

Now, we examine the PBG structures arising from the competition between the long range aperiodic order induced by the Thue-Morse and Double-Periodic structures. To do that, we have calculate the regions for forbidden frequencies (stop bands) as a function of the generations of Thue-Morse and Double periodic structures at parameters d_1 = 7 μm, d_2 = 3 μm and T = 300 K, and depicted in the figure 5.23(a) (Thue-Morse sequence) and 5.23(b) (Double-Periodic sequence). Although, the generation order and number of layers are similar corresponding to a given generation grows for both kinds of quasi-periodic structures, but layer arrangements are different as can see in table 5.1. Figures 5.23(a) and 5.23(b) show the distribution of the forbidden (black region) and allowed (white region) frequencies as a function of the generation of Thue-Morse and Double-Periodic sequences up to 6^{th} order, respectively. As expected, for large number of generation, we get large number of forbidden band gaps and allowed band regions become narrower and narrower as an indication of more localized modes. More forbidden band gaps appear at higher order Double-periodic generation in comparison to the Thue-Morse generation.

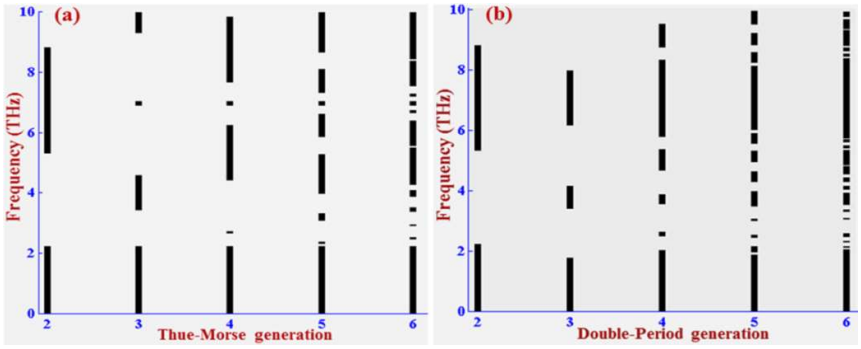

Figure 5.23 The distribution of the photonic bands as a function of (a) Thue-Morse generation and (b) Double-Periodic generation for 1-D quasi-periodic photonic crystal structures, where lattice parameters d_1 = 7 μm, d_2 = 3 μm and temperature T = 300 K.

Now, we investigate the effect of temperature on the PBGs in case of the Thue-Morse and Double-Periodic structures. Structural arrangements of the second order

quasi-periodic sequence are similar for Fibonacci, Thue-Morse and Double-periodic structure so here we choose 3rd and 4th order Thue-Morse and Double-Periodic sequences. Figures 5.24 (a and b) and 5.25 (a and b) show the reflection spectra as a function of the temperature for Thue-Morse ($(T_3)^{10}$ and $(T_4)^{10}$) and Double-periodic ($(D_3)^{10}$ and $(D_4)^{10}$) structures, respectively. The structures T_n and D_n represent the n^{th} order Thue-Morse and Double-Periodic structures, respectively. We can see from these figures, when increasing the temperature from 200 K to 360 K, the higher band edge of the first band gap shifts to higher frequency and the lower band edge is invariant. However, both the upper and lower band edges of the higher order band gaps shift to higher frequency, and bandwidth of these bands generally decrease as the increase of temperature. But, in case of the structure $(T_4)^{10}$ and $(D_4)^{10}$, bandwidth of the second order band gap initially decreases up to 280 K and then increases with temperature.

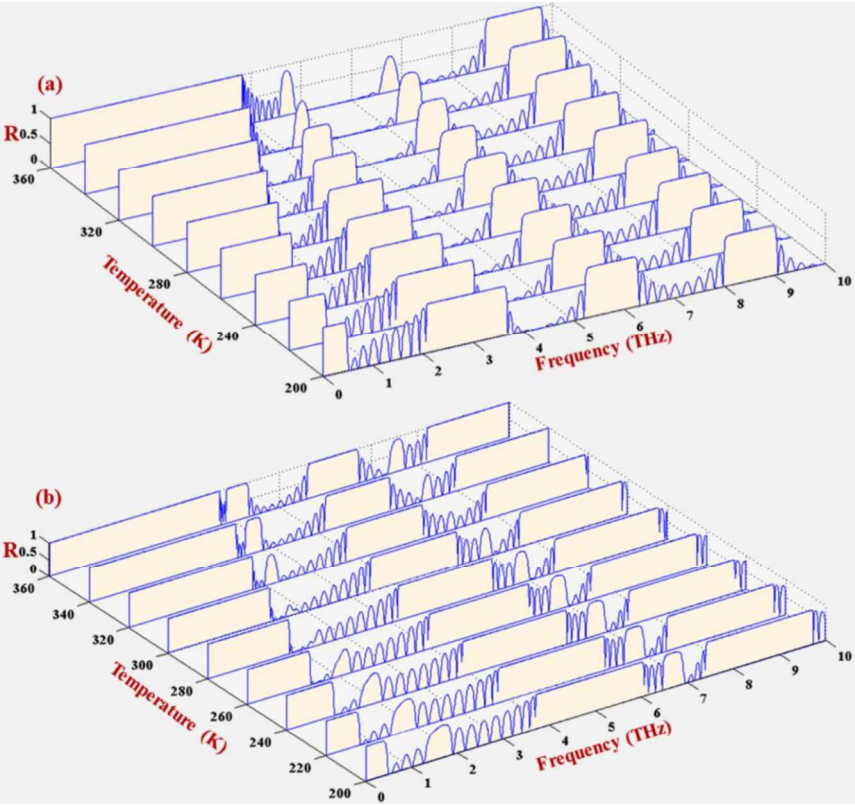

Figure 5.24 Reflectance (R) of the structure (a) $(T_3)^{10}$ and (b) $(T_4)^{10}$ as a function of frequency with varying temperature and assuming parameters $d_1 = 7$ μm and $d_2 = 3$ μm.

Now, we have emphasized the OBGs as changing the generation of Theo-Morse and Double-Periodic sequences. To do that, we have calculate the ubiquitous forbidden band regions for both TE and TM-polarization as a function of Theo-Morse and Double-Periodic generation for the parameters $d_1 = 7$ μm, $d_2 = 3$ μm and T = 300 K, and

depicted in the figures 5.26(a) (Thue-Morse sequence) and 5.26(b) (Double-Periodic sequence). Here, the black regions represent the OBGs. It is clearly shown that generally two OBGs observe, but for 4th order Thue-Morse generation and 3rd order Double-Periodic generation, we observe three OBGs.

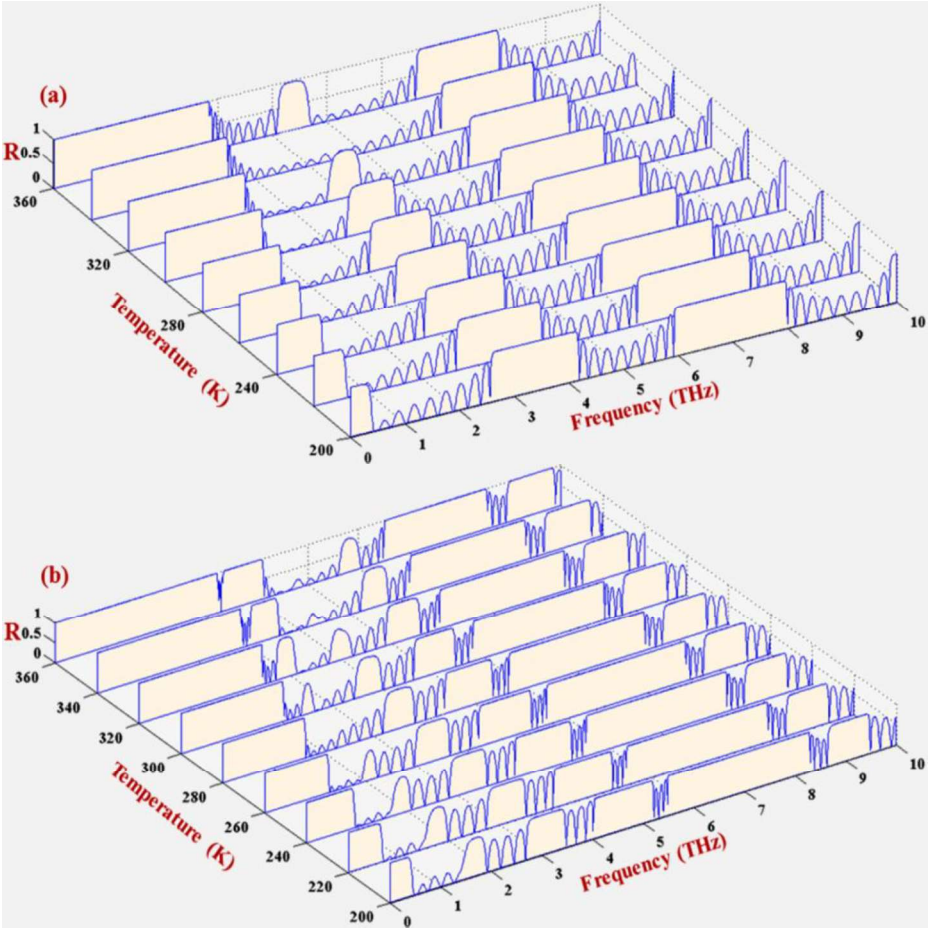

Figure 5.25 Reflectance (R) of the structure (a) $(D_3)^{10}$ and (b) $(D_4)^{10}$ as a function of frequency with the varying temperature, and assuming $d_1 = 7$ μm and $d_2 = 3$ μm.

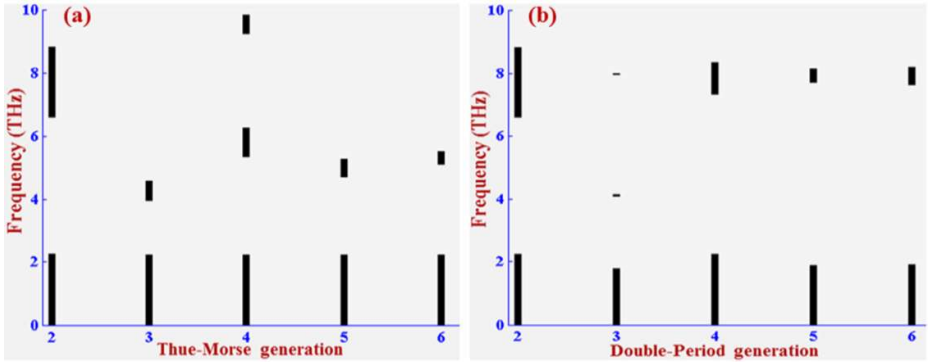

Figure 5.26 The distribution of omnidirectional band gaps as a function of (a) Thue-Morse and (b) Double-Periodic generation for 1-D quasi-periodic PCs structures, where lattice parameters $d_1 = 7$ μm, $d_2 = 3$ μm and temperature T = 300 K.

To discuss the effect of temperature on the OBGs in case of the Thue-Morse and Double-Periodic structures, we have plotted the distribution of OBGs as a function of the temperature in figure 5.27 (a and b) and 5.28(a and b) for the Thue-Morse (T_3 and T_4) and Double-periodic (D_3 and D_4) structures, respectively. Here, black regions represent the OBGs. It can see from these figures that the upper frequency limit of the first OBG shifts to higher frequency and their bandwidth becomes broader as increasing the temperature. While, both the upper and lower band edges of the higher order OBGs shift to higher frequency and the bandwidth of these gaps become narrow and narrow as the increase of temperature. In the case of the structure D_3, higher order OBGs disappear as increasing temperature above 300 K.

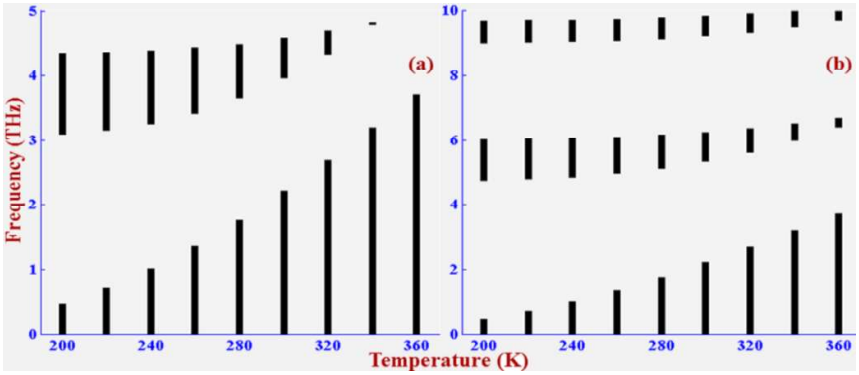

Figure 5.27 The distribution of omnidirectional bands as a function of temperature for the structures (a) $(T_3)^{10}$ and (b) $(T_4)^{10}$, where lattice parameters $d_1 = 7$ μm and $d_2 = 3$ μm.

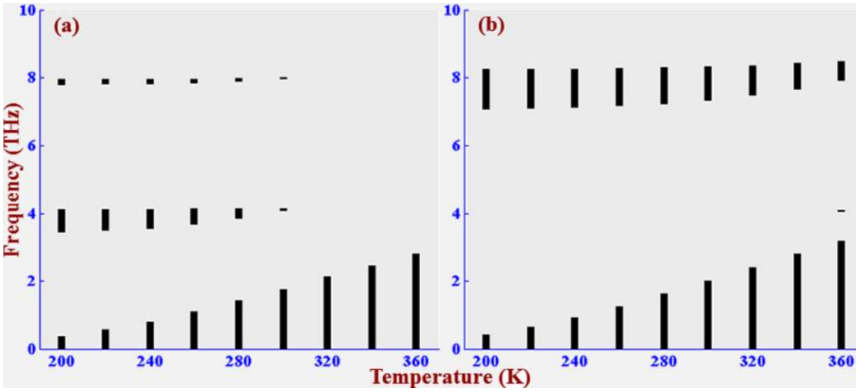

Figure 5.28 The distribution of omnidirectional bands as a function of temperature for the structures (a) $(D_3)^{10}$ and (b) $(D_4)^{10}$, here lattice parameters $d_1 = 7$ μm and $d_2 = 3$ μm.

Finally, we have investigated the distributions of the total photonic bandwidth and total omnidirectional bandwidth as a function of the generation of quasi-periodic (Fibonacci, Thue-Morse and Double-Periodic) sequence and temperature. Figures 5.29(a) and 5.29(b) show the total photonic bandwidth variation as a function of the quasi-periodic generation and temperature, respectively. Figure 5.29(a) shows that the

total photonic bandwidth increases with quasi-periodic generation for 3rd to 6th order. Total bandwidths are same for second order quasi-periodic generation since which is same of all considered quasi-periodic sequences. Total bandwidths for Double-Periodic multilayer structure are extremum at higher order generation. Figure 5.29(b) shows that the total photonic bandwidth of second order quasi-periodic (F_2 or T_2 or D_2) sequence linearly increases with temperature. However, total photonic bandwidth of third order Fibonacci (F_3) sequence initially increases and then decreases with the increase of temperature, and the total photonic bandwidth of third order Thue-Morse (T_3) and Double-Periodic (D_3) sequence randomly change with temperature. Total photonic bandwidth is maximum for second order quasi-periodic sequence at higher temperature.

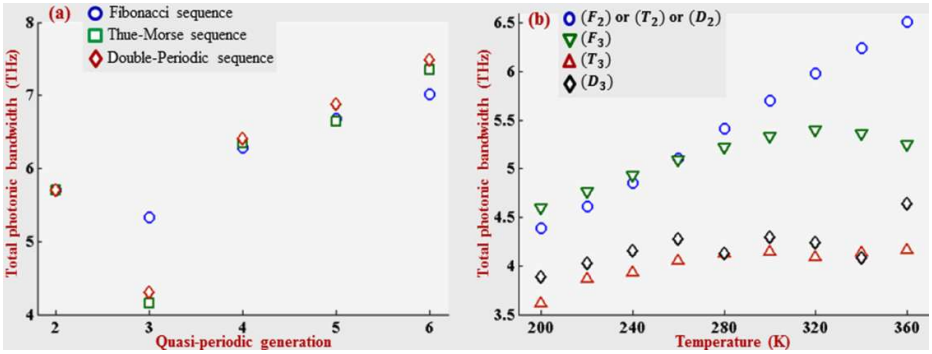

Figure 5.29 The variation of the total photonic bandwidth as a function of the (a) quasi-periodic generation and (b) Temperature in 1-D quasi-periodic multilayer structures, where lattice parameters; $d_1 = 7$ μm and $d_2 = 3$ μm.

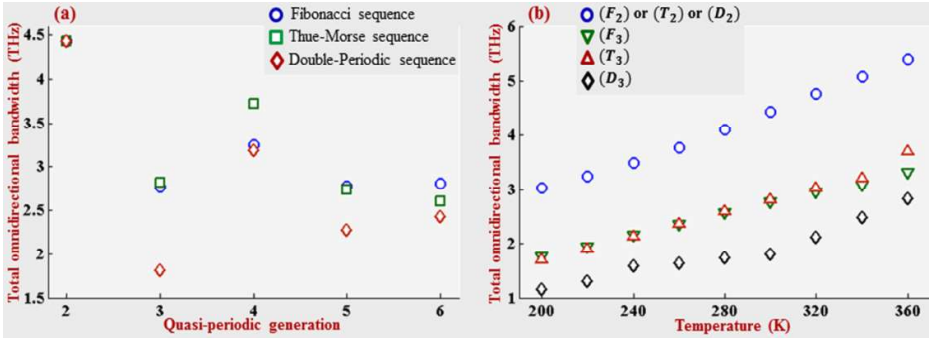

Figure 5.30 The variation of the total omnidirectional bandwidth as a function of the (a) quasi-periodic generation and (b) Temperature in 1-D quasi-periodic multilayer structures, where $d_1 = 7$ μm and $d_2 = 3$ μm.

The influences of quasi-periodic generation and temperature on the total omnidirectional bandwidth are shown in figures 5.30(a) and 5.30(b), respectively. The total omnidirectional bandwidths of the quasi-periodic (Fibonacci, Thue-Morse and Double-Periodic) structures randomly change with quasi-periodic generation and it is maximum for second order generation. The total omnidirectional bandwidth of the

second (F_2, T_2 and D_2) and third (F_3, T_3 and D_3) order quasi-periodic structures increases with increasing the temperature. We find that the total omnidirectional bandwidths of second order (F_2 or T_2 or D_2) quasi-periodic structures are extremum. However, in the case of third order quasi-periodic structures, total omnidirectional bandwidth is higher for F_3 and lower for D_3 structures. Thus, the temperature, lattice parameters and generation of quasi-periodic (Fibonacci, Thue-Morse and Double-Periodic) sequences have great influence on the photonic and omnidirectional band gaps of the proposed structures.

5.4 Conclusion

In this chapter, we have presented the influence of graded index materials and semiconductor on the PBG properties of 1-D quasi-periodic (Fibonacci, Thue-Morse and Double-Periodic) PC structures. In the case of the quasi-periodic structures with graded index materials, the number of PBG increases with layers thickness. We also observed that more and more PBGs and photonic localization modes appear with the generation of quasi-periodic sequences. The position of the localization modes and band gaps affect with grading profiles. Wider PBGs are observed in the case of maximum contrast of the refractive index of the constituted materials. Results may provide the basic understanding of the influence of the graded materials on the photonic modes and band gaps in the quasi-periodic PC structures. In the case of the quasi-periodic structures with semiconductors, lower order PBGs and OBGs of the structures strongly depend on the temperature, and their bandwidth increase with temperature. However, the band edges of higher order PBGs and OBGs shift to the higher frequency, and their bandwidth becomes narrower as the increase of temperature. With increasing the lattice parameters, the number of PBG increases, but the bandwidth of first order band gaps is invariant for fixed layer thickness ratio. Moreover, the frequency band region and bandwidth affect with Fibonacci, Thue-Morse and Double-Periodic sequences. Furthermore, total photonic and omnidirectional bandwidths can be tuned through the change of temperature and quasi-periodic generations and sequences. Accordingly, we can tune the PBGs and OBGs by tuning the temperature, lattice parameters, grading parameters and generation of quasi-periodic sequences and different types of quasi-periodic systems. Such tunable PBGs and OBGs of the proposed structures will offer to design mirrors, filters and optical sensors, and other optical devices.

★★★★★★